Article

A Revisited Mechanism of the Graphite-to-Diamond Transition at High Temperature

Sheng-cai Zhu, Xiao-zhi Yan, Jin Liu, Artem R. Oganov, Qiang Zhu

qiang.zhu@unlv.edu

HIGHLIGHTS

Both experiment and simulation were employed to study the graphite-diamond transition

The simulation suggests that diamond grows faster in graphite [120] than in [001]

This graphite-diamond interface model from simulation is consistent with experiments

The uncovered mechanism can be used to improve the synthetic diamond

We performed large-scale molecular dynamics simulations on the graphite-diamond transition under high-temperature, high-pressure conditions. The simulations suggested that diamond nuclei would emerge due to the corrugation and thermal fluctuation of graphite layers and then grow in a preferred direction along the graphite [120] direction, resulting in the cubic diamond phase being the kinetically favorable product while the hexagonal phase would appear as minor amounts of twin structures. The simulated coherent interface is confirmed by subsequent high-resolution transmission electron microscopy experiments.

Matter

Article

A Revisited Mechanism of the Graphite-to-Diamond Transition at High Temperature

Sheng-cai Zhu,[1,2] Xiao-zhi Yan,[3] Jin Liu,[4] Artem R. Oganov,[5] and Qiang Zhu[1,6,*]

SUMMARY

The graphite-diamond transition, under high-pressure and high-temperature conditions, has been a central subject in physical science. However, its atomistic mechanism remains under debate. Employing large-scale molecular dynamics (MD) simulations, we report a mechanism whereby the diamond nuclei in the graphite matrix propagate in two preferred directions, among which the graphite [120] is about 2.5 times faster than [001]. Consequently, cubic diamond (CD) is the kinetically favorable product, while only a few hexagonal diamonds (HDs) can exist as the twins of CDs. The coherent interface of t-(100)gr//(11-1)cd + [010]gr//[1-10]cd observed in MD simulation was confirmed by our high-resolution transmission electron microscopy experiment. The proposed mechanism not only clarifies the role of HD in graphite-diamond transition but also yields atomistic insight into strengthening synthetic diamond via microstructure engineering.

INTRODUCTION

Diamond, a stable form of carbon under high pressure, has been found naturally in the Earth's crust as a result of carbon's evolution at high-pressure and high-temperature (HPHT) conditions over the geological timescale.[1–3] Due to its many remarkable properties, diamond is in great demand in both industry and fundamental research.[4–7] However, at ambient conditions graphite is more stable than diamond (with a difference of ∼10 meV/atom from the modern quantum mechanical simulation based on density functional theory [DFT][8] and ∼17 meV/atom from more accurate diffusion Monte Carlo calculation[9]). Despite years of efforts, synthesizing diamond from graphite was not possible until the 1950s.[10,11] Due to the distinct structural packing between graphite and diamond, the transition generally needs to go through a rather complicated pathway at HPHT conditions (15–18 GPa and 1,500°C–2,300°C).[5,12–15] Fabricating diamond from other precursors, such as amorphous carbon,[16] carbon nanotubes,[17] and carbon nanoparticles,[15] has also been considered. It was reported that controlling the microstructure of diamond, such as nanotwinning, is key in promoting the product's mechanical properties.[18] However, due to the lack of fundamental understanding of atomistic mechanism in these phase transitions, it remains challenging to realize a truly rational control of the product's microstructure during the process of synthesis.

Experiments show that cubic diamond (CD) is the main product under HPHT conditions.[19,20] However, another metastable form, hexagonal diamond (HD, also known as Lonsdaleite), was also observed in meteorites,[21,22] shockwave experiments,[23,24] and computer simulations.[25] Several experiments suggested that HD is the

Progress and Potential

The graphite-diamond phase transition is a central subject in physical science. Among the debates after many years of studies, one outstanding issue is the role of hexagonal diamond (HD), which was argued to be the preferable product according to the simulation but never reported in the compression experiments on graphite under high-pressure and high-temperature (HPHT) conditions. From a synergy between experiment and simulation, we investigated the atomistic mechanism of the graphite-diamond transition in HPHT conditions. Our study suggests that the growth of diamond has a preferred direction, which notably favors the formation of cubic diamond (CD). On the other hand, HD only appears as the twin structures of CD. We further investigated the possibility of harvesting the twin structures via microstructure engineering, which may have the potential to advance the fabrication process in the synthetic diamond industry.
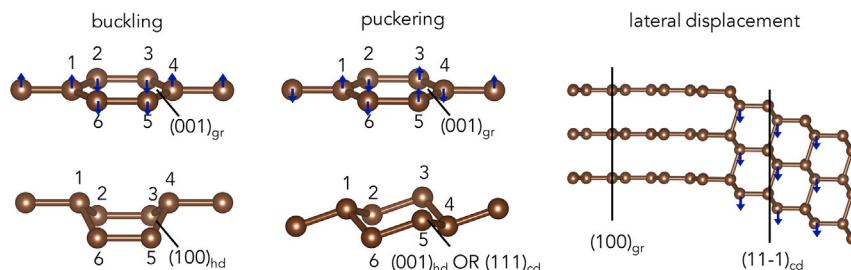
Figure 1. Atomistic Mechanisms of Graphite-to-Diamond Transition
From left to right: buckling, puckering, and lateral displacement.

intermediate phase of graphite-to-diamond transition[26,27] based on a few newly observed X-ray diffraction (XRD) peaks. However, the assignment of new XRD peaks to HD is not well accepted due to the blurry nature of the pattern.[28–31] In a recent study, Németh et al. reported that the HD cannot be obtained as a discrete material but only can be present as diamond {111} stacking fault or diamond (113) twins.[32] Thus, there is still no consensus that HD can be synthesized as a discrete material from the static compression of graphite. In addition to diffraction, electron microscopic techniques have been employed to study the graphite-diamond transition. A recent transmission electron microscopy (TEM) experiment suggested that graphite transforms to diamond without any intermediate phases but through two coherent interfaces between graphite and CD, namely (100)gr//(11-1)cd and (001) gr//(111)cd.[33] Following the orientation relationship, the coherent interface can be uniquely defined by the relation between specific planes and directions of two crystals on either side of the boundary. Thus, they can be expressed by two parallel crystal planes $(hkl)a//(h'k'l')b$ and two parallel directions $[uvw]a$ and $[u'v'w']b$, where $[uvw]$ and $[u'v'w']$ lie in the (hkl) and $(h'k'l')$ planes. Wheeler and Lewis[20] found that the shock-quenched diamond contains both CD and HD domains with orientations of (100)gr//(11-1)cd + [010]gr//[1-10]cd and (100)gr//(001)hd + [010]gr//[010]hd, respectively. They proposed that the phase transition can be achieved by the displacement of adjacent pairs of <−120> row with relative shears on alternating graphite basal planes. Despite these encouraging successes, collecting and interpreting the diffraction and TEM data under HPHT conditions remains challenging in general.

Complementary to the experimental studies, atomistic simulations can access a broader pressure-temperature space and provide insights into the phase transition at atomic level. In the past, several possible pathways have been proposed,[25,34–36] including puckering, buckling, and lateral displacement mechanisms[37–41] (as summarized in Figure 1), among which the puckering mechanism was suggested in many studies. For example, Fahy et al.[34,35] proposed that graphite (001) plane would transform to the chair architecture of CD (111) or HD (001) plane under compression. In this mechanism, the interplanar distance in graphite first collapsed, leading to a puckering of the graphitic basal planes. The puckered planes then suddenly undergo an electronic reconfiguration from sp^2 to sp^3 state. The whole large graphite (001) plane puckers and transforms to CD (111) or HD (001) layer by layer homogeneously.[42] Similar to puckering, the buckling mechanism suggests that the graphite (001) plane will transform to the boat architecture of HD (100) and then complete the entire transition to HD. In a recent work, Xie et al.[26] suggested that this mechanism yielded the lowest energy-barrier pathway by the state-of-the-art transition-state sampling method. Unlike the collective motion in either buckling or puckering, the lateral displacement mechanism requires a group of carbon

[1]Department of Physics and Astronomy, University of Nevada, Las Vegas, NV 89154, USA

[2]School of Materials, Sun Yat-sen University, Guangzhou 510275, China

[3]Academy for Advanced Interdisciplinary Studies and Department of Physics, Southern University of Science and Technology, Shenzhen 518055, China

[4]School of Mechanical Engineering, Jingchu University of Technology, Jingmen 44800, China

[5]Skolkovo Institute of Science and Technology, 3 Nobel Street, Moscow 143026, Russia

[6]Lead Contact

*Correspondence: qiang.zhu@unlv.edu

https://doi.org/10.1016/j.matt.2020.05.013

CellPress

atoms belonging to adjacent graphite sheets stochastically vibrating out of a graphite basal layer (up or up/down) and thus transforming to CD or HD. Via first-principles molecular dynamics (MD) simulation, Scandolo et al.[36] found that graphite transits to CD while HD exists as the twin of CD. Interestingly, the preferred orientation relation from their MD simulation can be interpreted as (100)gr//(11-1)cd + [010]gr//[1-10]cd. Tateyama et al.[42] also found that a similar mechanism is preferred when a large strain is allowed. Using an artificial neural network (ANN) potential, Khaliullin et al.[25] carried out a large-scale atomistic simulation to study the energetics of the nucleation mechanism of the graphite-diamond phase transition. To obtain the nucleus energies, they seeded diamond nuclei inside a graphite matrix ($\sim$100 × 100 × 100 Å) and optimized the geometry by constant-pressure MD simulations at 1,000 K for 30 ps to relax the atoms around the constrained region. Khaliullin's work provided an important first step toward understanding the nucleation mechanism of graphite-diamond transition in bulk at the atomistic level. However, using the ANN potential to perform an HPHT MD simulation on a large cell ($\sim$10-50 nm) at the timescale of nanoseconds is still beyond our computational capability. Therefore, the mechanism of graphite-diamond phase transition under realistic HPHT conditions remains elusive.

To our knowledge, most of the theoretical results were from the simulations based on small structural models under the assumption of homogeneous nucleation. When using the periodic boundary conditions, the entire (001)gr basal layer will turn into (111)cd, (001)hd, or (100)hd. However, the minimum number of atoms required to trigger such a transition (nuclear core) is unknown. Therefore, the calculated energy barriers for a periodic unit cell may not be instructive in evaluating the kinetic preference of different transition pathways under consideration. For instance, HD formation was calculated to be preferred over CD formation due to such energy-barrier comparison,[26] which is contrary to the experimental observations. To our knowledge, the current state of the art in determining the energy barrier based on DFT is reliable, but the small periodic unit cell may not be suitable for describing the entire graphite-to-diamond phase transition, since graphite is a system with strongly anisotropic behavior. To account for such an effect a large simulation model is needed, while most of the previous studies have been restricted to simulation cells with only a few tens of atoms. Finally, in a realistic model, the graphite sheet is supposed to depart from the equilibrium state due to thermal fluctuation under finite temperature and local stress. Recently, Gao et al.[43] reported that the grain boundaries play an important role in the graphite-to-diamond phase transition. Therefore, these previously reported mechanisms in a small unit may be limited in describing the transitions occurring in HPHT conditions.

To fully understand this underlying phase-transition mechanism, we conducted a complete study at different scales. First, we revisited the most likely graphite/diamond interface models under compression through an exhaustive sampling of small periodic unit cells. Second, we carried out a series of large-scale MD simulations based on a newly developed angular dependent potential (ADP) to gain an atomistic understanding of the diamond nucleation and growth under HPHT conditions. Our MD simulations demonstrated that the nuclei emerge at the graphite grain boundaries. Strikingly, we found that the commonly believed [001]gr direction is not the only preferred growth direction; instead, the propagation of diamond along [120]gr with the crystallographic orientation t-(100)gr//(11-1)cd + [010]gr//[1-10]cd is much faster. Following this mechanism, CD is the main product while HD can exist as the twinning structure. The coherent interface resolved from high-resolution TEM (HRTEM) images is consistent with our MD simulation. Findings from this study
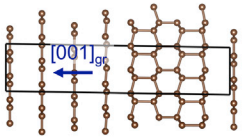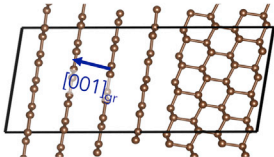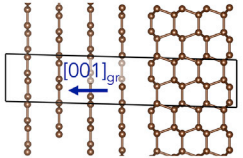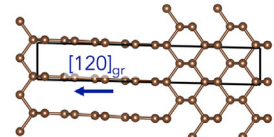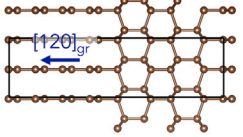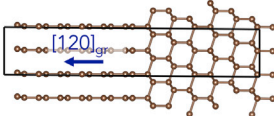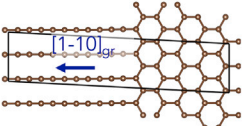
Name	Interface structure	OR	Ea	γ	Name	Interface structure	OR	Ea	γ
GH1		$(001)_{gr}//(001)_{hd}$ $[010]_{gr}//[010]_{hd}$	0.31	0.39	GC1		$(001)_{gr}//(111)_{cd}$ $[010]_{gr}//[1\text{-}10]_{cd}$	0.28	0.37
GH2		$(001)_{gr}//(100)_{hd}$ $[010]_{gr}//[010]_{hd}$	0.16	0.19	GC2		$(100)_{gr}//(010)_{cd}$ $[010]_{gr}//[101]_{cd}$	0.19	0.19
GH3		$(100)_{gr}//(001)_{hd}$ $[010]_{gr}//[010]_{hd}$	0.29	0.31	GC3		$(100)_{gr}//(11\text{-}1)_{cd}$ $[010]_{gr}//[1\text{-}10]_{cd}$	0.35	0.36
GH4		$(110)_{gr}//(100)_{hd}$ $[1\text{-}10]_{gr}//[001]_{hd}$	0.22	0.21					

Figure 2. Summary of the Possible Phase-Transition Path of Graphite to Diamond from Small Unit Cell Simulation, Including Their Interface Models, Orientation Relationship (OR), Energy Barrier (Ea in eV/Å^2), and Interface Energy (gamma in eV/Å^2)

The propagation directions are marked by blue arrows. The propagation direction of GH1, GH2, and GC1 is [001]gr; propagation direction of GH3, GC2, and GC3 is [120]gr; propagation direction of GH4 is [1-10]gr.

shed light on the long-standing debates around graphite-to-diamond phase transition, and facilitate understanding of the anisotropic behavior of the (001)gr plane under HPHT conditions. In addition, we propose a route to fabricate superhard diamond by harvesting the twin structures along [120]gr at the microstructural level via the pre-bent graphite sheets.

RESULTS

Transition-State Sampling under Static Conditions

We started our investigation by scanning the low-energy intermediate interface models of graphite and diamond. To explore them exhaustively, we visited more than 10,000 energy minima by the stochastic surface walking (SSW) method[44–46] together with the high-dimensional neural networks (NN) potential.[47] The sizes used in the simulation models range from 12 to 126 atoms per unit cell. Among them, seven lowest interface energy structures between graphite/CD and graphite/HD were extracted for further analysis in detail (Figure 2). The atomic structure information of those interfaces and the relative transition pathway can be found in Supplemental Information (see details in Data S1). They were named according to the transition products with different interfacial energies, namely GH1 (0.39 eV/Å^2), GH2 (0.19 eV/Å^2), GH3 (0.31 eV/Å^2), GH4 (0.21 eV/Å^2), GC1 (0.37 eV/Å^2), GC2 (0.19 eV/Å^2), and GC3 (0.36 eV/Å^2). By inspecting their geometries, we found that alignment of HD domain in GH1 is 90° off relative to that in GH2, GC2 is 54.75° off relative to GC3, while GH2 and GH3 have the same crystal orientation but different coherent planes.

Clearly, all three previously proposed mechanisms have been covered by these interface models. For instance, GH1 and GC1 follow the puckering mechanism

Matter
Article

CellPress

whereby the flat (001)gr transforms to chair architecture of HD and CD, respectively, while GH3 follows the buckling mechanism whereby (001)gr transforms to the boat architecture of (100)hd plane. In these models, diamond is supposed to grow along the direction perpendicular to graphite sheets. On the other hand, GH3, GH4, GC2, and GC3 follow the lateral displacement mechanism. In detail, GH3, GC2, and GC3 can be obtained by carbon atoms vibrating out of the (001)gr plane of graphite in [010]gr view while GH4 is in [1-10]gr view. Since the CD (111)cd plane and HD (001)hd plane have similar transition mechanism and atomic arrangements, they can coexist and form a hybrid interface, namely GH3/GC3, as Xie et al. reported.[26] Our results are largely consistent with those structures found by Xie et al., except that we found two new interface structures between graphite and CD, namely GC2 ((100)gr//(010)cd + [010]gr//[101]cd) and GC3 ((100)gr//(11-1)cd + [010]gr// [1-10]cd). It should be noted that GC3 is very similar to the fragment of a mixed phase (GCH) proposed by Xie et al.[26] However, these authors failed to provide the entire GC3 model due to the limit of simulation model size. Indeed, the GC3 interface structure was observed by Wheeler and Lewis[20] in their shockwave experiment. This also marks the importance of performing the simulation with a sufficiently large model.

For the suggested pathways, it is important to investigate their energy barriers during the graphite-diamond transition. The average energy barriers of the puckering mechanisms GH1 and GC1 are 0.31 eV/Å^2 and 0.28 eV/Å^2, respectively. GH2 has the lowest barrier, 0.16 eV/Å^2. For the lateral displacement mechanism (GH4 and GC2), carbon atoms just need to shift by one-half of the interlayer with the energy barriers 0.22 eV/Å^2 and 0.19 eV/Å^2, while GH3 and GC3 need to overcome higher energy barriers (0.29 eV/Å^2 and 0.35 eV/Å^2) by shifting one-third of the interlayer.

Direct Modeling of the Phase Transition from Large-Scale MD Simulations

These atomic interface models are instructive in understanding the possible atomistic mechanism of the graphite-diamond transition. However, they are limited by the size of simulation model and cannot describe the phase transition under realistic conditions. To overcome these limits, we employed large-scale MD simulations to directly study this phase transition under the relevant HPHT conditions. In this study, both the single-crystalline and polycrystalline graphite models were considered. Simulations were carried out in the NPT (isothermal-isobaric) ensemble with incremental pressures. MD simulations probe only sufficiently fast and frequent processes. First-order phase transitions such as graphite to diamond typically have a high activation barrier, and can only be seen by MD at pressures or temperatures exceeding those of equilibrium phase transition. Therefore, we used the excessive pressure to accelerate the phase transition in our MD simulation. To begin with, both the single-crystal system (150,000 atoms) and polycrystal system (1,226,000 atoms, composed of several grains with randomly generated orientations) were relaxed at 25 GPa and 1,500 K with sufficiently long equilibration time of 0.20 ns. The pressure was then steadily increased until the phase transition was observed. After a few test runs, we optimized the final pressures at 40 GPa for polycrystal and 80 GPa for single crystal with compression rate 5 GPa/ns and 16.66 GPa/ns, which allowed us to study the phase transition at lower critical pressure conditions with affordable simulation cost.

A typical MD trajectory of polycrystalline graphite under compression is recorded in animation (Videos S1 and S2) and depicted in Figure 3. Clearly, the nuclei were initiated by the local (001)gr plane distortion at the graphite's grain boundaries, followed by the propagation along different directions. We can better understand
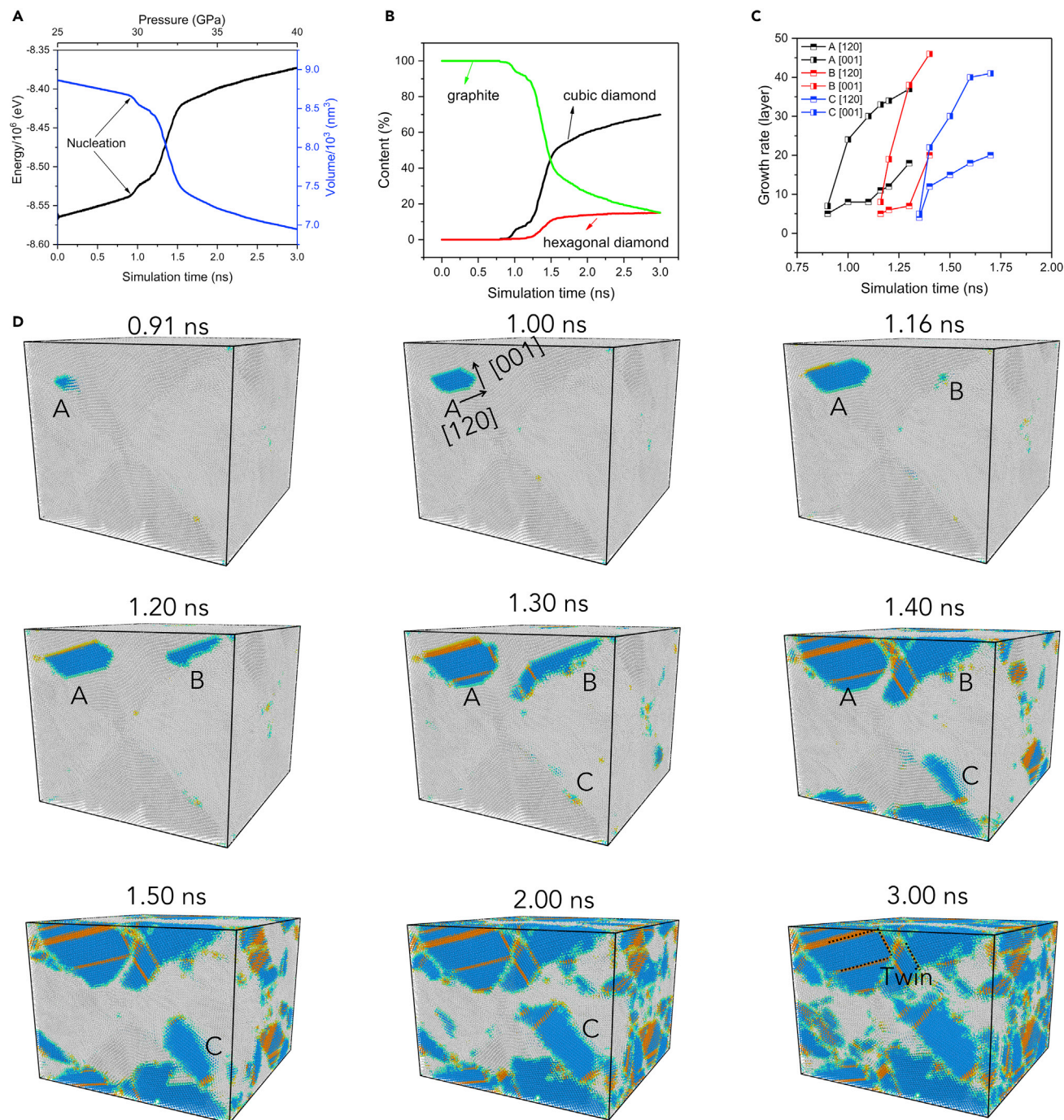
Figure 3. Statistical Analysis of MD Simulation

(A) Energy and volume curves as a function of the simulation time.

(B) Growth rates of graphite, cubic diamond, and hexagonal diamond during the simulation time.

(C) Anisotropic phase-transition behavior of A, B, and C domains in [120]gr and [001]gr directions.

(D) List of representative snapshots at different intermediate stages of simulation. In the snapshots, the atoms representing graphite, cubic diamond, and hexagonal diamond are marked by gray, blue, and orange, respectively.

the entire trajectory from the evolution of several key thermodynamic quantities such as energy and volume (Figure 3A). The entire process can be split into three stages. At the first stage (<0.9 ns), the energy (volume) of the system smoothly increases

Matter
Article

CellPress

(decreases). When it reaches a critical pressure (29 GPa), there is a dramatic change of the slope, signaling the formation of diamond nuclei and their propagation in the graphite matrix (0.9–1.6 ns). Finally, the system reaches a stage without significant structural change (>1.6 ns). Note that there still exists a notable fraction of untransformed graphite in the system, in agreement with previous experimental observations that the graphite-diamond transition could not be completed in a short time period.

We also analyzed the statistics in each MD snapshot. As shown in Figure 3B, we found that the ratio of carbon atoms in the graphite pattern steadily decreased while the ratio of CD atoms increased with time. Interestingly, we also observed a certain ratio of atoms labeled as HD, which appeared after the formation of nucleation of CD (0.91 ns versus 1.21 ns). Combining the detailed image analysis (Figure 3D), we found that HD exists as twinning structures (fewer than four layers), which were randomly located in the CD matrix. Thus, HD should be better interpreted as a by-product during the growth of CD in the graphite matrix. Although several previous experiments suggested that HD is the intermediate phase of graphite-to-diamond transition[26,27] based on a few newly observed XRD peaks, the assignment of new XRD peaks to HD is still controversial. From thorough analysis of HRTEM experiments, Németh et al.[32] suggested that HD exists as twinning structures. Here, our MD simulation provides the direct theoretical evidence to support Németh's observations.

Obviously, the growth of diamond nuclei exhibits a strong anisotropic behavior. At the beginning, the shapes of nuclei were nearly sphere-like (see Figure 3D). Later, we found that diamond propagated quickly along the [120]gr direction after the formation of nuclei while the growth along [001]gr direction was slower (Figure 3C). We also selected three different diamond nuclei (marked A, B, and C in Figure 3D) from the simulation and monitored their growth as a function of time. In general, the growth rate of (100)gr//(11-1)cd is about 2.5 times that of (001)gr//(111)cd. This is contrary to the previous results based on the small simulation models at zero temperature,[25,34,35] which suggests that the preferred growth direction is either [001]gr or [120]gr. The high-strain graphite on (100)gr//(11-1)cd interface with smaller d spacing is unstable, which is why the propagation along the [120]gr direction is much faster. Therefore, the entire transition should follow a hybrid mechanism involving growth at both lateral and normal directions of the graphite sheets.

Our simulation also differs from the previous DFT simulations in terms of the interface geometry. In the MD simulation, we observed that the graphite (001) in the interface structure (Figure 3D) is slightly tilted compared with the ideal (001) plane. This leads to a non-orthogonal dihedral angle of 70.5° between the tilted graphite (001) and diamond (11-1) planes, which agrees well with the experimental observation (to be discussed in the following section). Therefore, we name this interface t-(100)gr//(11-1)cd + [010]gr//[1-10]cd. Note that the tilted graphite (001) plane will return to the ideal alignment under the geometry optimization in both DFT and force-field calculations at 0 K. It also should be mentioned that the general lateral displacement mechanism allows the formation of phase-growth propagation frontiers with high index planes. If the diamond nuclei propagate along [120]gr with different rates, different phase-growth propagation frontiers will occur, as shown in Figures 4E and S3. In this case, other high index twins or stacking faults may occur when these high index planes meet highly bent graphite during the phase propagation. On the other hand, at high temperature, strong thermal fluctuation can introduce a pronounced corrugation to the planar graphite sheet and thus change the
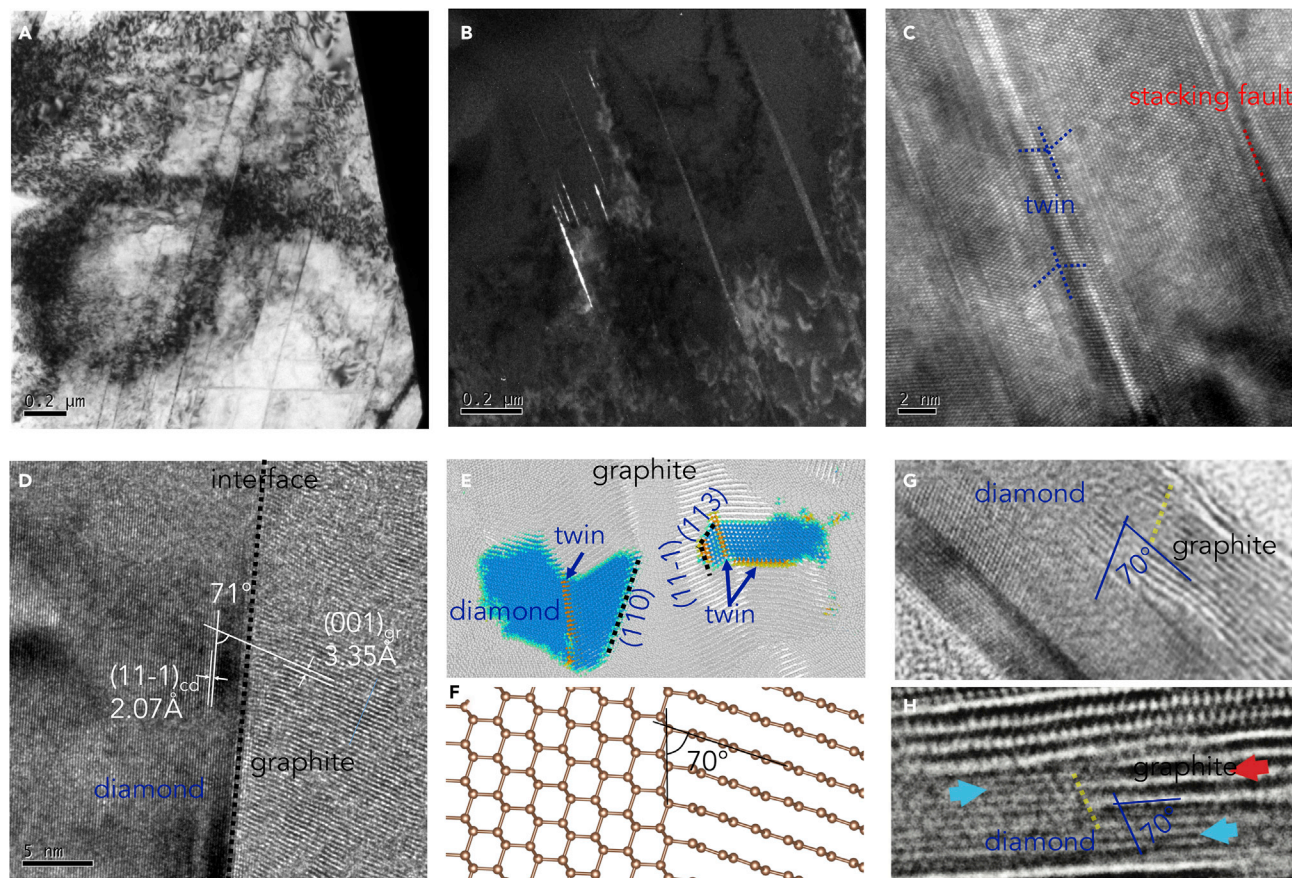
⌀ CelPress

Matter
Article

Figure 4. TEM Image Analysis

(A–C) TEM images of cubic diamond. (A) Selected area electron diffraction. (B) Dark-field TEM. (C) The twin structure and stacking fault are highlighted.

(D) HRTEM image of phase junction between graphite and diamond.

(E) Phase junction slab from MD simulation of the polycrystalline system.

(F) Junction from the small cell simulation.

(G and H) The experimental phase junction from Le Guillou et al.[29] (G) and Garvie et al.[33] (H), both with t-(100)gr//(11-1)cd + [010]gr//[1-10]cd and (001) gr//(111)cd + [010]gr//[1-10]cd interface. The yellow dotted lines were drawn to emphasize the region of graphite-diamond phase boundary. Copyright 2007, with permission from Elsevier (G); Copyright 2014, with permission from Mineralogical Society of America (H).

geometry significantly. Therefore, large-scale modeling at high temperature is necessary to describe the entire transition at the atomic level.

We also repeated the MD calculation with faster compression rate for both polycrystalline (poly 2: 10 GPa/ns) and single-crystalline (single: 16.66 GPa/ns) samples. For the polycrystalline sample with faster compression rate, no significant differences in the transformation path were observed except that the transition pressures were slightly shifted to a higher value. For the single crystals, the critical pressure is much higher (60 GPa), which is expected since the single crystal has no defects to facilitate nucleation.

Experimental Verification

To verify the simulation results, we conducted a series of experiments. Polycrystalline diamond was synthesized at HPHT and processed by focused ion beam (FIB). Furthermore, the samples were analyzed by TEM. From the low-magnification TEM image, we find that the main product is CD, which is consistent with our simulation (Figures 4A and 4B). Also, the dark-field TEM and HRTEM images suggest that

Matter
Article

CellPress

HD is the stacking fault (twinning) structure of CD (Figures 4B and 4C). The HRTEM images of the sample in Figure 4D can easily distinguish the mixture of graphite and diamond. Specifically, the observed d-spacings of 3.35 and 2.07 Å are graphite (001) plane and diamond (111) plane, respectively. The dihedral angles between the graphite t-(001) and diamond (11-1) in the interface of t-(100)gr//(11-1)cd + [010] gr//[1-10]cd is 71 ($\pm$1)°. Considering the fluctuation of graphite (001) plane, the measured dihedral angle is very close to the results from our MD simulation ($\sim$70°) (see the interface model in Figures 4E and 4F). Although the (001)gr//(111)cd + [010]gr//[1-10]cd interface has been observed often, the interface on (100)gr plane (Figures 4G and 4H) has been rarely reported.[29,33] This could probably be explained by the fact that the transition along the [120]gr direction is much faster and thus less likely to be captured by an *ex situ* experiment. The identification of the t-(100)gr//(11-1)cd + [010]gr//[1-10]cd interface is essential for us to understand the complete picture for this transition.

Besides the HRTEM from our own experiment, two main interface models, defined as GC1 (001)gr//(111)cd and t-GC3 (100)gr//(111)cd, were also reported in the previous literature[29,33] (Figures 4G and 4H). For example, viewing along the [1-10]cd direction, two {111} diamond fringes can be found in Figures 4G and 4H, and the (100)gr is coherent to (111)cd with a dihedral angle of $\sim$71($\pm$1)° between (001)gr and (111)cd. Moreover, the GC1 interfaces were found six times, while there exists only one GC3 interface structure in Garvie et al.[33] This can be explained by the fact that the growth along [120]gr is much faster than that along [001]gr. Once (100)gr//(11-1)cd interfaces form, they quickly propagate along [120]gr and eventually transform to diamond. The relative occurrences of two interface structures support the identified preferred propagate directions observed in our MD simulation.

DISCUSSION

In the past, the graphite-to-diamond phase transition was mostly suggested to follow either the puckering or buckling mechanism, whereby both prefer the growth of CD/HD from graphite in a layer-by-layer manner along the [001]gr direction. However, both our MD simulation and TEM analysis suggested that there should exist two preferred crystal growth directions, i.e., [120]gr and [001]gr. In fact, the growth along [120]gr is even faster than along [001]gr. This can be understood by the classical nucleation theory,[37,48] which expresses the thermodynamic potential change (ΔG) on forming the nucleus as

$$\Delta G = n\left[\Delta g(p, T) + E_\varepsilon\right] + \gamma S, \qquad \text{(Equation 1)}$$

where n is the number of molecules in the nucleus, $\Delta g(p, T) = g_\beta - g_\alpha$ is the difference in specific thermodynamic potentials (per molecule) between the initial (α) and the new (β) phases, E_ε is the strain energy (per molecule) in the matrix-nucleus system after nucleation, γ is the specific energy of the interphase boundary, and S is the interfacial area. The kinetic preference can be quantified by $\frac{\partial \Delta G}{\partial n}$. Since (100)gr//(11-1)cd and (001)gr//(111)cd have a similar specific interface energy (γ, see the DFT results), the nucleation growth is dominated by strain energy term (E_ε). To obtain a quantitative understanding, we selected two typical interface models GC1 and GC3 with half diamond and half graphite in the superlattice. If diamond grows along [001]gr, the penalty energy $\frac{\partial \Delta G}{\partial n}$ due to lattice distortion can be described by the strain energy of GC3. On the other hand, the strain energy of GC1 denotes the corresponding $\frac{\partial \Delta G}{\partial n}$ for the growth along [120]gr (see Figures 5D and 5E). According to our calculation,
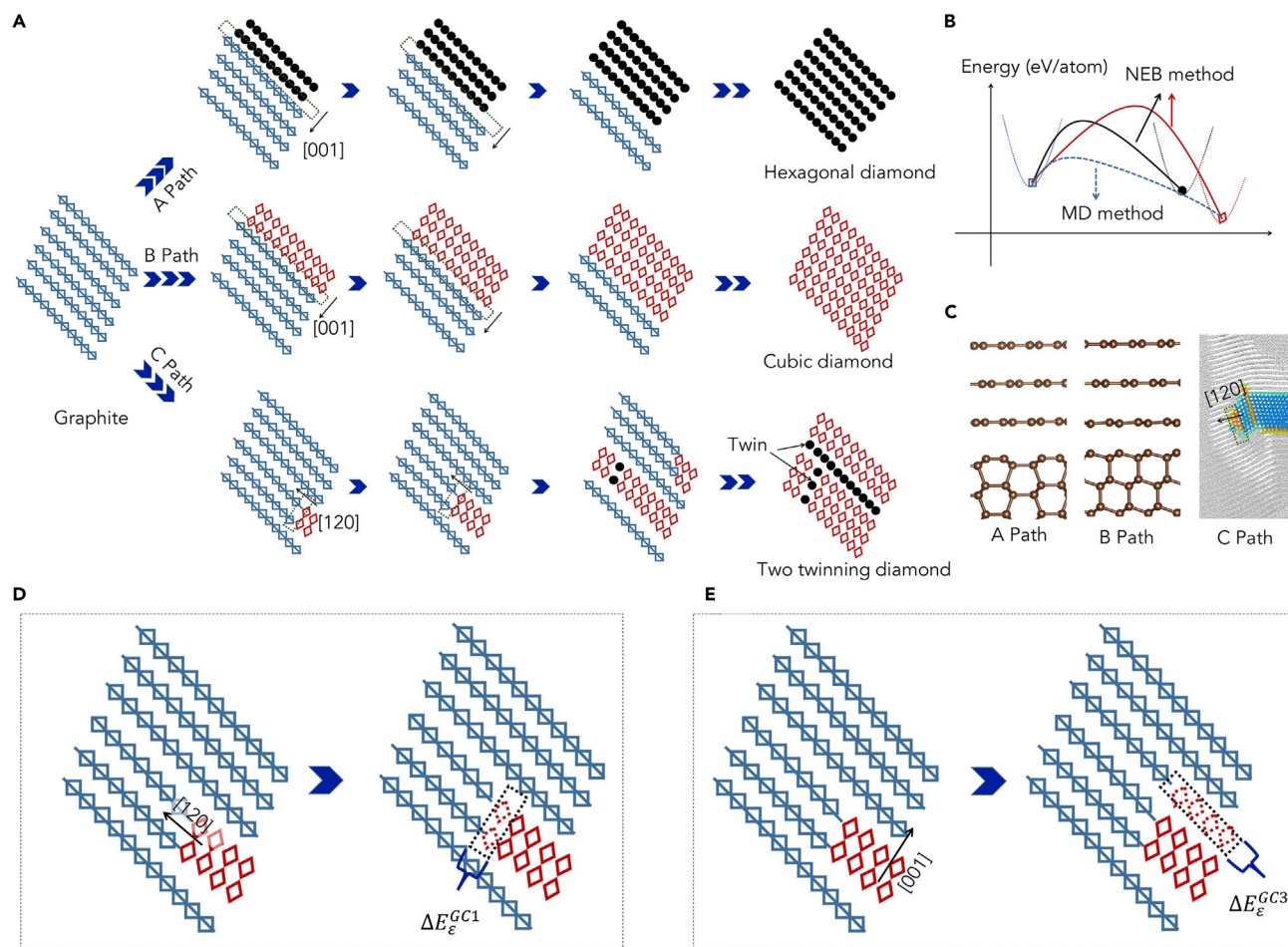
CellPress

Matter
Article

Figure 5. Schematic Phase-Transition Mechanisms

(A) Schematic representation of nucleation and growth of the graphite to CD and HD, including graphite-to-HD transition and growth in [001]gr direction (A path, top), graphite-to-CD transition and growth in [001]gr direction (B path, middle), and graphite-to-CD transition with HD along both [120]gr and [001] directions (C path, bottom).

(B) Schematic energy-barrier comparison for different paths (A, black; B, red; C, dotted).

(C) Interfaces constructed from the different paths.

(D) Penalty strain energy for [120]gr direction growth $\Delta E_\varepsilon^{GC1}$.

(E) Penalty strain energy for [001]gr direction growth $\Delta E_\varepsilon^{GC3}$.

$$E_\varepsilon = \frac{[E_{\text{distorted}}(\text{gr}) - E_{\text{ideal}}(\text{gr})] + [E_{\text{distorted}}(\text{CD}) - E_{\text{ideal}}(\text{CD})]}{N}. \quad \text{(Equation 2)}$$

For the 128-atoms GC1 model the total strain energy is merely 9 meV/atom, and the 32-atoms GC2 total strain energy is 93 meV/atom, whereas the strain energy is 184 meV/atom for the 96-atoms GC3 model. It is important to note that the models of GC1 and GC3 only account for two special cases where there exist half diamond and half graphite. Hence, the calculated E_ε values and propagation rate will vary during the growth of diamond. From our MD simulation, we found the overall growth along [120]gr is 2.5 times faster than [001]gr. In real experiments the ratio may be even larger, since t-(100)gr//(11-1)cd + [010]gr//[1-10]cd interface was seldom identified. Despite this numerical variation, we can safely conclude that the [120]gr growth is kinetically more favorable than [001]gr growth due to a notable difference between the strain energies.

Matter
Article

CellPress

The mechanism can also reconcile the long debates on the role of HD in the graphite-diamond transition. In our simulation, we exclude the possibility of HD as the intermediate phase between graphite-to-diamond transition under HPHT conditions. HD can exist at twin boundaries of CD during the growth of CD nuclei. It is interesting to probe the formation of twins along both directions. When two CD nuclei meet along the [001]gr direction, they would stochastically form either stacking fault, a twin boundary, or perfect conjunction. On the other hand, the formation of twins along [120]gr largely depends on the local corrugation of graphite sheets involved in the transition. As shown in Figure 4E, the twins tend to appear where the graphite sheets are locally bent. When graphite sheets are bent, forming the twin structure is apparently the best way to minimize the total penalty energy due to lattice mismatch. Thus, introducing the corrugation to the graphite sheet is a key to producing the twins. In our MD simulation, the HPHT conditions, together with the local structural defects (i.e., grain boundaries), provide the sources to bend the graphite sheets and thus produce the twins along [120]gr. Similar results were also found in several other experiments[29,33] and MD simulations.[49] In particular, a recent experiment,[18] through starting from another precursor of carbon onion nanoparticles, also reported the presence of many twins in two different directions (Figure S4). This can be well understood by the fact that the graphite sheets in the carbon nanoparticles have been pre-bent to adopt the onion-like arrangement.[18] Note that it is much more difficult to produce the [120]gr direction twins if the graphite sheets adopt a purely planar configuration. For instance, many synthetic diamonds from single-crystal graphite were reported to have the lamellar texture with only one direction of twin structures along the [001]gr direction in a nanodomain[5,50] (Figure S5). As a result, the carbon nanoparticles with pre-bent microstructure can enhance the production of twins along the [120]gr direction, which thus promote the hardness of the synthetic diamond.

Let us summarize our findings for the graphite-to-diamond phase transition under HPHT conditions. While previous studies suggested that the growth of diamond has only one preferred direction [001]gr (paths A and B in Figure 5A), our results showed that graphite transforms to CD with two preferred growth directions ([001]gr and [120]gr, path C in Figure 5A), with [120]gr being more favorable. The defects developed at graphite's grain boundaries help to trigger the formation of CD nuclei. The growth along [120]gr is generally faster than along [001]gr due to the anisotropic strain distribution at the graphite/CD interfaces. Following this mechanism, the HD will appear when two CD nuclei meet in these two main growth directions. In particular, the occurrence of diamond twins along [120]gr is determined by the local configuration of graphite sheets involved in the phase transition. Therefore, the mechanism developed here can be used to tailor the mechanical properties of diamond by controlling its microstructure during the synthesis.

Conclusion

In summary, combining both large-scale MD simulation and HRTEM measurement, we propose a new graphite-to-diamond phase transition mechanism that can resolve several long-standing issues. We found that the graphite-to-diamond transition under HPHT conditions involves two preferred growth directions in which the growth of nuclei along the [120]gr direction is faster than that along the [001]gr direction due to an anisotropic distribution of interfacial strains. The coherent interface orientation relation resolved from HRTEM, t-(100)gr//(11-1)cd + [010]gr//[1-10]cd, confirmed the growth along [120]gr observed in our MD simulation. Following this mechanism, CD is the main product while HD is present as the twin boundary. This mechanism is also supported by previous results whereby two interface

structures were found and the observation of twin structures in two different directions ([120]gr and [001]gr). The results of this work rationalize that the graphite-to-diamond transition is largely rooted in the anisotropic behavior of the (001) plane and also suggest a route to fabricate the twin structures along [120]gr by pre-bending the graphite sheets. Understanding this mechanism can help better engineer the microstructure of synthetic diamonds from HPHT conditions, which has been demonstrated to have a great impact on mechanical properties such as hardness of the resulting diamond.

EXPERIMENTAL PROCEDURES

Resource Availability

Lead Contact

All questions should be addressed to qiang.zhu@unlv.edu.

Materials Availability

Commercially available high-purity well-crystallized graphite (99.99%, Alfa Aesar, Ward Hill, MA) with particle size of 5–20 μm was used as the starting material.

Data and Code Availability

This research employed several different computational methods. The details are given in the followingsection, Computational Details. The data generated from this research are available upon request by email.

Experimental Synthesis and Characterization

Polycrystalline diamond was synthesized from graphite under HPHT conditions. Graphite was pressed into a pellet and processed in a two-stage multi-anvil apparatus based on a DS6 × 25 MN cubic press machine. Samples were compressed to the desired values before heating, then heated at 1,400°C–2,000°C for 0.5–2 h at 14 GPa. The pressure was estimated by the well-known pressure-induced phase transitions of Bi, ZnTe, and ZnS. The treating temperature was directly measured by using W97Re3-W75Re25 thermocouples. After cooling to room temperature, the samples were prepared by FIB and characterized with a high-resolution transmission electron microscope (FEI Tecnai G2F20 S-Twin, operated at 200 kV).

Computational Details

Reaction Pathway Sampling

To explore the potential energy surface (PES) of carbon under high pressure, we employed the recently developed SSW method, which integrated with first-principles DFT method (SSW-DFT)[44–46] and the high-dimensional NN potential[47] to sample the low-energy interfaces and pathways. The SSW reaction pathway sampling is based on the SSW global optimization method, which is able to explore complex PES to simultaneously identify both structures and reaction pathways. For solid-phase transitions, this is to identify the one-to-one correspondence for lattice ($L(e_1,e_2,e_3)$, e_i being the lattice vector) and atom (q_i, $i = 1, .. 3N$, N being the number of atoms in cell) from one crystal phase (the initial state, IS) to another (the final state, FS), which constitutes the reaction coordinates of the reaction, i.e., $Q_{IS}(L,q) \rightarrow Q_{FS}(L,q)$. In one SSW pathway sampling simulation, we need to collect as many as possible IS/FS pairs (typically a few hundred) to ensure the identification of the best reaction coordinate, the one corresponding to the lowest energy pathway. With such a pair of reaction coordinates, $Q_{IS}(L,q)$ and $Q_{FS}(L,q)$, it is then possible to utilize the variable-cell double-ended surface walking (VC-DESW) method[46] to identify the reaction transition state and the minimum energy pathway.

Matter
Article

CellPress

The SSW pathway sampling is fully automated and divided into three stages in simulation, namely: (1) pathway collection via extensive SSW global search; (2) pathway screening via fast DESW pathway building; and (3) lowest energy pathway determination via DESW transition-state search. The first stage is the most important and most time-consuming part, which generates all the likely pairs of generalized reaction coordinates linking different crystal phases. For the carbon phase transition in this work, we have collected more than 1,000 pairs $Q\alpha(L,q)$ and $Q\beta(L,q)$, which leads to the finding of the lowest energy pathway. The lowest energy pathway obtained from sampling was then analyzed to identify the key atom displacement patterns. Using this information, we then further enlarged the supercell up to 60–126 atoms per cell via the interface intermediate structure mechanism (dependence on the interface structure) and re-searched the lowest energy pathway, which is found to dramatically lower the overall reaction barrier. The stability of the interfaces was evaluated by considering the interfacial energy,[51] defined as $\gamma = (E_{tot} - E_a - E_b)/2S$, where S is the interfacial area, E_a and E_b are the energies of the parent phases, and E_{tot} is the energy of the mixed phase.

DFT Simulations

For each image generated from SSW sampling, the energy and forces were calculated by the plane-wave DFT program VASP (Vienna Ab initio Simulation Package).[52] The electron-ion interaction of C atoms was represented by the projector augmented wave[53] scheme and the exchange-correlation functional utilized was GGA-PBE (generalized gradient approximation-Perdew-Burke-Ernzerhof).[54] The self-consistent field was regarded converged when the total (free) energy change and the band structure energy change between two steps were both smaller than 10^{-5} eV. For all the structures, both lattice and atomic positions were fully optimized in SSW-DFT/DFT until the maximal stress component was less than 0.1 GPa and the maximal force component less than 0.01 eV/Å.

Molecular Dynamics Simulation

To enable the large-scale MD simulation, we developed an interatomic potential for elemental carbon. Since the phase transition involves the break and formation of covalent bonds, an embedded atom model formalism with ADP was employed to fit the potential energy landscape of carbon based on massive DFT data. The details of the carbon-ADP potential will be published elsewhere. To validate the accuracy of the ADP potential, we calculated the equation of states for both graphite and diamond and compared them with the results from DFT (Figure S1). In addition, the energy barriers calculated by DFT and the ADP potential are consistent with each other, which indicate that the accuracy of ADP potential is sufficient for the purpose of this study (Figure S2). More details can be found in Supplemental Information. All MD simulations were run in the LAMMPS code.[55] In our calculation, three different initial models (one single-crystalline and two polycrystalline graphite models) were used. For the single-crystalline sample, there are 150,000 carbon atoms of graphite structure in a box with $a = 11$ nm, $b = 12$ nm, and $c = 10$ nm. In the bigger polycrystalline graphite model, we generated four grains randomly oriented in a ~23.4-nm cubic box with total ~1,226,000 atoms. In the smaller polycrystalline model, about 20 small grains were randomly oriented in a ~20-nm cubic box with total ~840,000 atoms. All initial geometries were heated to 1,500 K at 25 GPa for an equilibration of 0.2 ns. The constantly increasing pressures with a damping value of 1.0 were then applied to these samples for 3.0 ns. To understand the process, we chose to output the enthalpy, pressure, volume, and atomic structures every 1 ps. Simulations were carried out in the NPT ensemble, and a thermostat was employed to maintain a constant temperature with the damping constants of 0.2 ps on

Matter
Article

temperature and 1 ps on pressure. The simulation results, including the detection of CD/HD phase regions, were visualized and analyzed using the OVITO package.[56]

AUTHOR CONTRIBUTIONS

Q.Z. and S.-C.Z. conceived the research idea. S.-C.Z. performed the calculations. Q.Z. and S.-C.Z. analyzed the simulation data. X.-Z.Y. and J.L. collected the experimental data. All the authors contributed to interpretation and discussion of the data. S.C.-Z., A.R.O., and Q.Z. wrote and revised the manuscript.

These authors contributed equally: S.-C.Z., X.-Z.Y., and J.L.

DECLARATION OF INTERESTS

The authors declare no competing interests.

REFERENCES

1. Richardson, S.H., Gurney, J.J., Erlank, A.J., and Harris, J.W. (1984). Origin of diamonds in old enriched mantle. Nature 310, 198–202.

2. Stachel, T., and Harris, J.W. (2009). Formation of diamond in the Earth's mantle. J. Phys. Condens. Matter 21, 364206.

3. Walter, M.J., Kohn, S.C., Araujo, D., Bulanova, G.P., Smith, C.B., Gaillou, E., Wang, J., Steele, A., and Shirey, S.B. (2011). Deep mantle cycling of oceanic crust: evidence from diamonds and their mineral inclusions. Science 334, 54–57.

4. Liu, J., Zhan, G., Wang, Q., Yan, X., Liu, F., Wang, P., Lei, L., Peng, F., Kou, Z., and He, D. (2018). Superstrong micro-grained polycrystalline diamond compact through work hardening under high pressure. Appl. Phys. Lett. 112, 061901.

5. Isobe, F., Ohfuji, H., Sumiya, H., and Irifune, T. (2013). Nanolayered diamond sintered compact obtained by direct conversion from highly oriented graphite under high pressure and high temperature. J. Nanomater. 2013, 1–6.

6. Friel, I., Geoghegan, S.L., Twitchen, D.J., and Scarsbrook, G.A. (2010). Development of high quality single crystal diamond for novel laser applications. In Proceedings of SPIE, Vol. 7838, C. Lewis, D. Burgess, R. Zamboni, F. Kajzar, and E.M. Heckman, eds. (International Society for Optics and Photonics). https://doi.org/10.1117/12.864981.

7. Jenei, Z., O'Bannon, E.F., Weir, S.T., Cynn, H., Lipp, M.J., and Evans, W.J. (2018). Single crystal toroidal diamond anvils for high pressure experiments beyond 5 megabar. Nat. Commun. 9, 3563.

8. Selli, D., Baburin, I.A., Martoňák, R., and Leoni, S. (2011). Superhard s p 3 carbon allotropes with odd and even ring topologies. Phys. Rev. B 84, 161411.

9. Shin, H., Kang, S., Koo, J., Lee, H., Kim, J., and Kwon, Y. (2014). Cohesion energetics of carbon allotropes: quantum Monte Carlo study. J. Chem. Phys. 140, https://doi.org/10.1063/1.4867544.

10. Hall, H.T. (1960). Ultra-high-pressure, high-temperature apparatus: the "Belt". Rev. Sci. Instrum. 31, 125–131.

11. Bundy, F.P., Hall, H.T., Strong, H.M., and Wentorf, R.H. (1955). Man-made diamonds. Chem. Eng. News 33, 718.

12. Ohfuji, H., and Kuroki, K. (2009). Origin of unique microstructures in nano-polycrystalline diamond synthesized by direct conversion of graphite at static high pressure. J. Mineral. Petrol. Sci. 104, 307–312.

13. Sumiya, H., and Irifune, T. (2007). Hardness and deformation microstructures of nano-polycrystalline diamonds synthesized from various carbons under high pressure and high temperature. J. Mater. Res. 22, 2345–2351.

14. Sumiya, H., and Harano, K. (2012). Distinctive mechanical properties of nano-polycrystalline diamond synthesized by direct conversion sintering under HPHT. Diam. Relat. Mater. 24, 44–48.

15. Najiba, S., Juhl, S.J., Mandal, M., Liu, C., Durygin, A., Chen, J., Fei, Y., Alem, N., and Landskron, K. (2019). Synthesis of nanopolycrystalline mesoporous diamond from periodic mesoporous carbon: mesoporosity increases with increasing synthesis pressure. Scr. Mater. 162, 350–354.

16. Onodera, A., Higashi, K., and Irie, Y. (1988). Crystallization of amorphous carbon at high static pressure and high temperature. J. Mater. Sci. 23, 422–428.

Matter
Article

17. Yusa, H. (2002). Nanocrystalline diamond directly transformed from carbon nanotubes under high pressure. Diam. Relat. Mater. 11, 87–91.

18. Huang, Q., Yu, D., Xu, B., Hu, W., Ma, Y., Wang, Y., Zhao, Z., Wen, B., He, J., Liu, Z., et al. (2014). Nanotwinned diamond with unprecedented hardness and stability. Nature 510, 250–253.

19. Irifune, T., Kurio, A., Sakamoto, S., Inoue, T., Sumiya, H., and Funakoshi, K.I. (2004). Formation of pure polycrystalline diamond by direct conversion of graphite at high pressure and high temperature. Phys. Earth Planet. Inter. 143, 593–600.

20. Wheeler, E.J., and Lewis, D. (1975). The structure of a shock-quenched diamond. Mater. Res. Bull. 10, 687–693.

21. Hanneman, R.E., Strong, H.M., and Bundy, F.P. (2006). Hexagonal diamonds in meteorites: implications. Science 155, 995–997.

22. Frondel, C., and Marvin, U.B. (1967). Lonsdaleite, a hexagonal polymorph of diamond. Nature 214, 587–589.

23. Erskine, D.J., and Nellis, W.J. (2002). Shock-induced martensitic transformation of highly oriented graphite to diamond. J. Appl. Phys. 71, 4882–4886.

24. Erskine, D.J., and Nellis, W.J. (1991). Shock-induced martensitic phase transformation of oriented graphite to diamond. Nature 349, 317–319.

25. Khaliullin, R.Z., Eshet, H., Kühne, T.D., Behler, J., and Parrinello, M. (2011). Nucleation mechanism for the direct graphite-to-diamond phase transition. Nat. Mater. 10, 693–697.

26. Xie, Y.P., Zhang, X.J., and Liu, Z.P. (2017). Graphite to diamond: origin for kinetics selectivity. J. Am. Chem. Soc. 139, 2545–2548.

27. Britun, V.F., Kurdyumov, A.V., and Petrusha, I.A. (2004). Diffusionless nucleation of lonsdaleite and diamond in hexagonal graphite under static compression. Powder Metall. Met. Ceram. 43, 87–93.

28. Pokhilenko, N.P., Litasov, K.D., Ohfuji, H., Yamashita, T., Irifune, T., Isobe, F., and Afanasiev, V.P. (2015). Natural occurrence of pure nano-polycrystalline diamond from impact crater. Sci. Rep. 5, 1–8.

29. Le Guillou, C., Brunet, F., Irifune, T., Ohfuji, H., and Rouzaud, J.N. (2007). Nanodiamond nucleation below 2273 K at 15 GPa from carbons with different structural organizations. Carbon N. Y. 45, 636–648.

30. Yarosh, V.V., Danilenko, A.I., Britun, V.F., Kurdyumov, A.V., and Zelyavskii, V.B. (2012). The influence of the shock compression conditions on the graphite transformations into lonsdaleite and diamond. J. Superhard Mater. 34, 19–27.

31. Nakamuta, Y., and Toh, S. (2013). Transformation of graphite to lonsdaleite and diamond in the Goalpara ureilite directly observed by TEM. Am. Mineral. 98, 574–581.

32. Németh, P., Garvie, L.A.J., Aoki, T., Dubrovinskaia, N., Dubrovinsky, L., and Buseck, P.R. (2014). Lonsdaleite is faulted and twinned cubic diamond and does not exist as a discrete material. Nat. Commun. 5, 1–5.

33. Garvie, L.A.J., Németh, P., and Buseck, P.R. (2014). Transformation of graphite to diamond via a topotactic mechanism. Am. Mineral. 99, 531–538.

34. Fahy, S., Louie, S.G., and Cohen, M.L. (1986). Pseudopotential total-energy study of the transition from rhombohedral graphite to diamond. Phys. Rev. B 34, 1191–1199.

35. Fahy, S., Louie, S.G., and Cohen, M.L. (1987). Theoretical total-energy study of the transformation of graphite into hexagonal diamond. Phys. Rev. B 35, 7623–7626.

36. Scandolo, S., Bernasconi, M., Chiarotti, G.L., Focher, P., and Tosatti, E. (1995). Pressure-induced transformation path of graphite to diamond. Phys. Rev. Lett. 74, 4015–4018.

37. Britun, V.F., and Kurdyumov, A.V. (2000). Mechanisms of martensitic transformations in boron nitride and conditions of their development. High Press. Res. 101–111, https://doi.org/10.1080/08957950008200933.

38. Kurdyumov, A.V., Britun, V.F., and Petrusha, I.A. (1996). Structural mechanisms of rhombohedral BN transformations into diamond-like phases. Diam. Relat. Mater. 5, 1229–1235.

39. Gruber, T., and Grüneis, A. (2018). Ab initio calculations of carbon and boron nitride allotropes and their structural phase transitions using periodic coupled cluster theory. Phys. Rev. B 98, 1–19.

40. Zhou, X.-F., Qian, G.-R., Dong, X., Zhang, L., Tian, Y., and Wang, H.-T. (2010). Ab initio study of the formation of transparent carbon under pressure. Phys. Rev. B 82, 134126.

41. Dong, X., Zhou, X.-F., Qian, G.-R., Zhao, Z., Tian, Y., and Wang, H.-T. (2013). An Ab initio study on the transition paths from graphite to diamond under pressure. J. Phys. Condens. Matter 25, 145402.

42. Tateyama, Y., Ogitsu, T., Kusakabe, K., and Tsuneyuki, S. (1996). Constant-pressure first-principles studies on the transition states of the graphite-diamond transformation. Phys. Rev. B Condens. Matter 54, 14994–15001.

43. Gao, Y., Ma, Y., An, Q., Levitas, V., Zhang, Y., Feng, B., Chaudhuri, J., and Goddard, W.A. (2019). Shear driven formation of nano-diamonds at sub-gigapascals and 300 K. Carbon N. Y. 146, 364–368.

44. Shang, C., and Liu, Z.-P. (2013). Stochastic surface walking method for structure prediction and pathway searching. J. Chem. Theor. Comput. 9, 1838–1845.

45. Shang, C., Zhang, X.-J., and Liu, Z.-P. (2014). Stochastic surface walking method for crystal structure and phase transition pathway prediction. Phys. Chem. Chem. Phys. 16, 17845–17856.

46. Zhang, X.-J., and Liu, Z.-P. (2015). Variable-cell double-ended surface walking method for fast transition state location of solid phase transitions. J. Chem. Theor. Comput. 11, 4885–4894.

47. Huang, S.-D., Shang, C., Zhang, X.-J., and Liu, Z.-P. (2017). Material discovery by combining stochastic surface walking global optimization with a neural network. Chem. Sci. 8, 6327–6337.

48. Christian, J. (2002). The Theory of Transformations in Metals and Alloys (Pergamon).

49. Xie, H., Yin, F., Yu, T., Wang, J.-T., and Liang, C. (2015). Mechanism for direct graphite-to-diamond phase transition. Sci. Rep. 4, 5930.

50. Irifune, T., Kurio, A., Sakamoto, S., Inoue, T., and Sumiya, H. (2003). Ultrahard polycrystalline diamond from graphite. Nature 421, 599–600.

51. Zhu, S.C., Hu, Q., Mao, W.L., Mao, H.K., and Sheng, H. (2017). Hydrogen-bond symmetrization breakdown and dehydrogenation mechanism of FeO2H at high pressure. J. Am. Chem. Soc. 139, 12129–12132.

52. Kresse, G., and Furthmüller, J. (1996). Efficient iterative schemes for ab initio total-energy calculations using a plane-wave basis set. Phys. Rev. B 54, 11169.

53. Blöchl, P.E. (1994). Projector augmented-wave method. Phys. Rev. B 50, 17953–17979.

54. Perdew, J.P., Burke, K., and Ernzerhof, M. (1996). Generalized gradient approximation made simple. Phys. Rev. Lett. 77, 3865–3868.

55. Plimpton, S. (1995). Fast parallel algorithms for short-range molecular dynamics. J. Comput. Phys. 117, 1–19.

56. Stukowski, A. (2010). Visualization and analysis of atomistic simulation data with OVITO—the open visualization tool. Model. Simul. Mater. Sci. Eng. 18, 015012.